Vol. 354: 59–74, 2008
doi: 10.3354/meps07136

MARINE ECOLOGY PROGRESS SERIES
Mar Ecol Prog Ser

Published February 7

Generalised model of primary production in the southern Benguela upwelling system

Hervé Demarcq[1], Anthony J. Richardson[2,3], John G. Field[4,5,*]

[1]Institut de Recherches pour le Développement, CRH, BP 171, 34203 Sète Cedex, France
[2]Department of Mathematics, University of Queensland, St. Lucia, Queensland 4072, Australia
[3]Wealth from Oceans Flagship, CSIRO Marine and Atmospheric Research, Cleveland, Queensland 4163, Australia
[4]Marine Research Institute and Zoology Department, University of Cape Town, Rondebosch 7701, South Africa
[5]Marine Biological Association, Citadel Hill, Plymouth, PL1 2PB, UK

ABSTRACT: We provide a proof-of-concept demonstration using a novel method for estimating depth-integrated distributions of chlorophyll from archives of data from ships, buoys or gliders combined with remotely sensed data of sea surface temperature (SST) and surface chlorophyll *a* (chl *a*) from satellites. Our area of application has contrasting hydrographic regimes, which include the dynamic southern Benguela upwelling system and the stratified waters of the Agulhas Bank, South Africa. The method involves using self-organising maps (SOMs), a type of artificial neural network, to identify 'typical' chl *a* profiles regardless of their statistical form, provided several of a similar shape have been found in the training set. These are arranged in a linear array, ranging from uniform profiles low in chl *a* to profiles with high surface or subsurface peaks. We then use generalised modelling to relate these characteristic profiles to remotely sensed surface features, viz. surface chl *a* and SST, as well as area, season, and water depth (a proxy for distance offshore). The model accounts for 87% of the variability in chl *a* profile and is used to predict the type of profile likely for each pixel in monthly remote sensing composites of SST and surface chl *a* and then to estimate integrated chl *a* and primary production with the aid of a light model. Primary production peaks in mid-summer, reaching 5 mgC m^{-2} d^{-1} locally, with an average over the whole area and all seasons of 1.4 mg C m^{-2} d^{-1}. Seasonal variation is greatest in the southern part of the west coast, and lowest in the stratified southeast. Annual primary production for the southern Benguela region including the Agulhas Bank is ca. 156 million tC yr^{-1}. This is the most robust estimate of primary production in the Benguela system to date because it combines the spatial and temporal coverage provided by remote sensing with realistic vertical chl *a* profiles.

KEY WORDS: Remote sensing · SeaWiFS · Ocean colour · Primary production · Self-organising maps · SOM · Generalised additive model · SOM · Vertical chlorophyll *a* profile

INTRODUCTION

Marine phytoplankton play a major role in the global carbon cycle by fixing large quantities of atmospheric CO_2 and sequestering it to the bottom of the ocean. Phytoplankton also modify the surface of the oceans by absorbing light and heat energy, altering the physical and chemical properties of the surface ocean layers (Morel & Maritorena 2001). They also form the basis of marine food webs, which ultimately support all fisheries world-wide. In particular, phytoplankton play a crucial role in coastal upwelling areas characterised by short food webs; despite representing only 2 to 3% of marine areas and 8% of the global marine primary production (Antoine et al. 1996), they sustain 20 to 30% of global marine fisheries production (FAO 2005).

Remote sensing provides a powerful tool for measuring dynamic ocean properties synoptically, such as phytoplankton biomass and productivity (Longhurst 1995). Primary production can be estimated over large scales from the surface chlorophyll *a* (chl *a*) concentration and the surface solar irradiance through the use of photosynthesis models of various complexity (Morel & Berthon 1989, Platt & Sathyendranath 1993, Behrenfeld & Falkowski 1997). Although the performance of each model in estimating *in situ* production is not

*Corresponding author. Email: jgfielduct@gmail.com

related to their intrinsic complexity (Campbell et al. 2002), few of them directly incorporate information on the vertical distribution of phytoplankton.

Sensitivity analyses of primary production models (Platt & Sathyendranath 1988) show that the error in estimates of photosynthesis can be considerable when the chlorophyll maximum is near the surface. This is generally the case in coastal upwelling areas, where profiles are variable due to the wide range of oceanic conditions from active upwelling cells and filaments inshore to stratified waters offshore.

Several methods have been developed for describing non-uniform biomass profiles in the oceans. However, these methods tend to produce profile categories that are fixed for large spatial and temporal scales and may not be representative of the smaller scale variability in chl *a* profiles.

Recently, more flexible approaches using a suite of environmental variables have been used to estimate the shape of chl *a* profiles. Techniques such as self-organising maps (SOMs), a type of artificial neural network particularly adept at pattern identification (Kohonen 1997, Hewitson & Crane 2002, Richardson et al. 2003) have been used to identify limited sets of characteristic chl *a* profiles from archives of vertical chl *a* traces (Silulwane et al. 2001, Richardson et al. 2002). However, these studies did not use raw chl *a* profiles, but first parameterized the profiles using the shifted Gaussian model (Platt et al. 1988, Longhurst et al. 1995, Sathyendranath et al. 1995) and then based the SOM on these parameter values. This not only constrains the patterns identified to be Gaussian in shape, but the more unusual profiles that do not fit the shifted Gaussian model also have to be removed prior to analysis (e.g. ~15% of the profiles in Silulwane et al. [2001] and Richardson et al. [2002]). Another approach has been to use generalised modelling to estimate the 4 parameters of the shifted Gaussian model from several environmental variables (Richardson et al. 2003). These studies have had some success (r^2 of parameter values ranging from 15 to 74%) in predicting the subsurface shape of chl *a* profiles from predictors that can be estimated from satellite (sea surface temperature, SST; surface chl *a*) or are known (water column depth, season and location).

In the present study we develop a generic quantitative approach to derive primary production estimates using a simple light model and by describing the variation in vertical profile shape. We illustrate this approach by applying it to an area off southern South Africa that includes the dynamic upwelling cells of the southern Benguela region and the warm stratified conditions of the Agulhas system (Hardman-Mountford et al. 2003). Relatively few primary productivity estimates have been made in this region (but see Brown et al. 1991, Probyn et al. 1994, Carr et al. 2002), and none have used dynamically varying chl *a* profiles in their estimates. We first use self-organising maps to identify a limited set of generalised chl *a* profiles from an archive of nearly 2500 profiles in the region. We then use a generalised modelling approach to predict the characteristic chl *a* profiles from a suite of easily measured environmental variables. These are used to produce the most robust regional estimates of integrated chl *a* and primary production in the Benguela upwelling and Agulhas Bank systems to date.

MATERIALS AND METHODS

Collection of chlorophyll profiles. Oceanographic data were collected during fisheries surveys off the west and south coasts of South Africa (Fig. 1) by

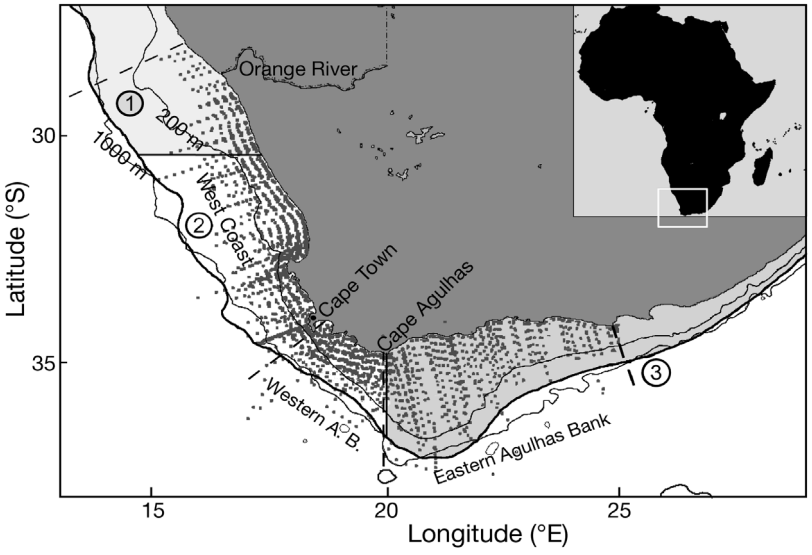

Fig. 1. Benguela and Agulhas systems showing sampling locations and bathymetry, with 200 m and 1000 m isobaths. Sub-areas used in the generalized model are eastern Agulhas Bank (EAB, east of 20° E), western Agulhas Bank (WAB, from 20° E to 34° S) and west coast (WCO, north of 34°S), delimited by dashed lines. Areas numbered 1 to 3 are those used to present the results of the remote sensing analyses. The Namaqua cell is included in Area 1, and the St. Helena Bay (32° S) and Cape Peninsula (33–34° S) cells plus the western Agulhas Bank (from Cape Point to Cape Agulhas, 18.5 to 20° E) are all in Area 2. The south coast includes the central and eastern Agulhas Bank (up to 29° E) and forms Area 3. The offshore limit used is the average position of the 0.5 mg m^{-3} surface chl *a* isopleth (thick black line); dots represent positions where ship's data was gathered

Marine and Coastal Management, Department of Environmental Affairs and Tourism, South Africa. Generally, each transect started 2 miles (1 statute mile = 1.609 km) from the coast, had stations 10 miles apart, and extended to the shelf-edge, although some transects were extended farther offshore. Fluorescence and temperature profiles were measured at each of 2500 stations down to 100 m or to within 5 m of the seabed (Fig. 1) by a thermistor and profiling fluorometer (Chelsea Instruments AquaTracka MKIII) between 1985 and 2002. Water samples were collected in Niskin bottles at the surface and at the depth of maximum fluorescence and assessed for chl *a* using standard techniques (Parsons et al. 1984).

Despite the well-known problems of using chl *a* as a surrogate for phytoplankton biomass (e.g. Cullen 1982, Legendre & Michaud 1999), we used it in this study because it is the biological variable most easily measured by satellite ocean colour (Morel & Berthon 1989, Sathyendranath & Platt 1993). The relationship between chl *a* and fluorescence is dependent upon the phytoplankton community present, which can change seasonally and spatially. We computed the linear relationship between extracted surface chl *a* ($\log_{10}$ transformed) and fluorescence separately for each cruise and for different areas within each cruise. High extracted surface chl *a* values corresponding to low fluorescence values measured by the fluorometer during the daytime were considered to be photo-inhibited (Cullen 1982, Cullen & Lewis 1995) and were excluded from the regression. Unfortunately, most of the shipboard data were collected before SeaWiFS data became available, and only 240 shipboard stations overlap with the ocean colour measurements.

Seasons were defined with a 1 mo lag from conventional seasons (e.g. summer: January to March) because of the lag in ocean response to atmospheric forcing. Three areas were defined (Fig. 1) based on their physical oceanographic characteristics and the number of shipboard observations available in each region. The west coast has seasonal upwelling, the western Agulhas Bank has some upwelling with a deep thermocline, and the eastern Agulhas Bank has a shallow thermocline. Depth of the water column was chosen to indicate the position in relation to the shore and continental shelf, and was estimated from the latitude and longitude of each profile using the latest General Bathymetric Chart of the Oceans (GEBCO) bathymetric chart release (IOC, IHO and BODC 2003).

Identification of characteristic profiles. The Self Organizing Map (SOM) is a dimension-reducing procedure whereby a multidimensional input is mapped onto a lower (usually 2-) dimensional continuous output space. The output space consists of a number of patterns characteristic of the data, with similar patterns neighbouring, and dissimilar patterns farther apart. As the output patterns resemble the input format, they are often more easily interpreted than data obtained using output from conventional multivariate techniques.

SOMs were applied to raw chl *a* profiles; thus, we did not need to exclude any profiles as was the case in previous studies. We first smoothed the profiles using a 3-point running mean and then interpolated these smoothed profiles at 1 m intervals. For profiles in water shallower than 100 m, a missing data code was used to make all input rows the same length (Kohonen et al. 1996). Missing data do not bias SOM results (Richardson et al. 2003). Thus, input data consisted of a table of the chl *a* at 100 depth intervals (columns) by the 2498 profiles (rows). The SOM was performed using the SOM_Pak software Version 3.1 for Windows (Kohonen et al. 1996), which is produced by and freely available from the Neural Network Research Centre at the Helsinki University of Technology (www.cis.hut.fi/research/som_lvq_pak.shtml). This procedure generates an array of generalised chl *a* patterns (Richardson et al. 2002). For more details on the SOM procedure, consult Kohonen (1997), Hewitson & Crane (2002) or Richardson et al. (2003). The step-by-step detailed presentation of the SOM method as applied to chl *a* profiles can be found in Richardson et al. (2002).

The SOM arranges the output of the analysis into a rectangular diagram of characteristic patterns. Each of the characteristic profiles has chl values for 100 depths. In the current analysis (see Fig. 2) we chose a 1D configuration of the rectangular topology (15 columns by 1 row). The 1D configuration rather than a 2D configuration was chosen to capture a continuum of change in the profile shape that could more easily be used to predict the characteristic profile from environmental variables (see information on generalised modelling in the following subsection). Both smaller and larger dimension maps were explored with similar results, but 15 nodes (i.e. 15 characteristic profiles) appeared to capture the variability in the profile shape adequately. Too many nodes do not adequately reduce the data to characteristic patterns, whereas too few nodes do not allow differentiation of underlying patterns.

To perform the SOM, a number of parameters need to be set. Various values of the learning rate, initial update radius, and the number of cycles were tested to determine the best overall map, with the best combination, in terms of the minimum overall error and, thus, the best fit to the input data, being a 2-step training process (Step 1: learning rate = 0.2, initial update radius = 3, number of cycles = 1000; Step 2: learning rate = 0.1, initial update radius = 0, number of cycles = 10 000). The SOM was randomly initialised and run 50 times to obtain the lowest quantisation error (a good-

ness-of-fit measure that minimises errors between the characteristic and raw profiles).

Predicting chl *a* profiles from environmental variables. To predict the characteristic profile (i.e. profile number 1 to 15) from a suite of easily measured environmental variables, we used a 2-step generalised modelling approach (see Richardson et al. 2003). In the first step, relationships between the 15 ordered characteristic profiles from the SOM and various surface observations collected with the profiles were assessed using Generalised Additive Models (GAMs). A GAM estimates the relationship between the response and each predictor, assuming no *a priori* form (Hastie & Tibshirani 1990). Such a non-linear approach was used because of the complex interaction of biology (e.g. physiological state and particular species present) and physics (e.g. shear between water parcels, currents) controlling the shape of profiles. Continuous predictor variables used were surface chl *a*, SST, and water column depth. Predictors were selected because they influence profile shape (Richardson et al. 2002) and can be measured from satellite (SST and surface chl *a* concentration) or are known (season, locality, and depth of water column). Two of these predictors were categorical, viz. season and area. The response (profile number) was treated as a continuous variable because of the relatively large number (15) of categories.

The response is modelled as a sum of smooth functions of the predictors using a Loess smoother (effectively a form of moving average). Upon visual inspection of normality and homoscedasticity, it did not appear necessary to transform the response. The GAMs were built using a backward stepwise approach using Akaike's Information Criterion to identify the most parsimonious model (MathSoft 2001). Although GAMs are good at characterising non-linear relationships through their use of smoothers, they do not provide a predictive equation (Hastie & Tibshirani 1990). Therefore, in the second step of the generalised modelling process we visually assessed the form of the relationship between profile number and each continuous environmental predictor by inspection of the GAM plots, and then parameterised these using piecewise linear regression. Categorical variables were parameterised in an identical fashion to the GAMs. Parameterisations were implemented as a Generalised Linear Model (GLM), producing a predictive equation.

Remote sensing data. Several types of remotely sensed data were used in this study. Surface chl *a* concentration data from September 1997 to August 2003 used in the generalised modelling and in the primary production model were extracted from the SeaWiFS Global Area Coverage (GAC) database (currently processed with the empirical OC4V4 algorithm; O'Reilly et al. 1998, Patt et al. 2003) using the SeaDAS software (Baith et al. 2001). The spatial resolution was kept at 4.5 km, and maps of monthly arithmetic averages were computed from daily level 2 images. To obtain decontaminated averages, a preliminary elimination of residual cloud contaminated pixels was performed using a multiple detection of pixels whose value is at least 3 times higher than the surrounding values in a 3×3 to 5×5 box.

A time series of monthly averages of the Photosynthetic Available Radiation (PAR, see oceancolor.gsfc.nasa.gov/DOCS/seawifs_par_algorithm.pdf) is used to consider the inter-annual variability of the incident light available for photosynthesis. This product is generated from the SeaWiFS top of the atmosphere radiances using standard procedures and statistical relationships (Frouin et al. 2003).

Monthly averages of SST used in the generalised modelling were computed from multi-daily METEOSAT infrared data over the same time period at a spatial resolution of 6 km. The lower resolution of the sensor (5 to 6 km), compared with the 4.5 km of GAC AVHRR data, is largely compensated by the higher frequency of observation that allows better cloud elimination (Demarcq & Citeau 1995).

Primary production. Comparisons of different models of primary production based on different assumptions regarding their spectral resolution have shown that the broad-band model of photosynthesis irradiance (*P*-*E*) gives realistic estimates of production (Kyewalyanga et al. 1992, Campbell et al. 2002). This model has a theoretically null bias for values of chl *a* around 2 mg m^{-3}, which is close to the average value found in the region. Primary production was calculated using a broad-band light transmission model proposed by Smith (1936) and used by others (e.g. Platt & Sathyendranath 1993, Carr 2002). The bio-optical model uses the vertical structure of biomass to estimate the attenuation coefficient of light with depth (k_d, hereafter referred to as k). The statistical uncertainty associated with the instantaneous measurement of light is largely subsumed by monthly averaging of individual daily SeaWiFS measurements at each pixel location. This is particularly suited to modelling the inter-annual variability of primary production.

Benguela waters are mostly of the Case 1 type (Morel et al. 2006), since there is minimal riverine inflow. Detailed studies of the relationships between k and the chl *a* concentration for Case 1 waters have been done by Morel (1988) and Giles-Guzman & Alvarez-Borrego (2000) whose average results are very close to the result of Riley (1956) that we use below. The resulting k values averaged from the 3 relationships in the 1 to 10 mg m^{-3} of chl *a* interval (typical values for our region) exhibit a coefficient of variation

of only 8% (4% in the 1 to 6 mg m^{-3} of chl *a* interval. The light calculation was performed each metre down to the euphotic depth, assumed to be where the PAR is 1% of its surface level.

The whole production model was then applied at every pixel location on each SeaWiFS monthly image for 6 yr from September 1997 to August 2003, and the profile estimated from the GLM relationship based on environmental predictors. According to the classification of primary production models by Behrenfeld & Falkowski (1997), our model belongs to the category of the time-integrated models (TIMs) in which depth is resolved, but both time and wavelength are integrated.

The primary production associated with a given photosynthetic biomass (P^B) can be expressed as:

$$P^B = \left(E, \alpha^B, P^B_m\right) \quad (1)$$

where α^B is the initial slope of the *P-E* curve (in mgC chl^{-1} h^{-1} [µmol m^{-2} s^{-1}]$^{-1}$), *E* is irradiance and P^B_m the light-saturated rate of photosynthesis normalized to chlorophyll (in mgC chl^{-1} h^{-1}). Both parameters are determined from *in situ* measurements. The full function can be expressed by:

$$P(z) = [B(z)\alpha^B E(z)] \Big/ \sqrt{1 + [\alpha^B E(z) / P^B_m]} \quad (2)$$

P(z) represents primary production and *B*(z) biomass, as a function of depth; the light at a given depth *z*, *E*(z), is expressed as a decreasing exponential function of the light at the sea surface (representing the PAR). We use the relationship first proposed by Riley (1956) and used by Nelson & Smith (1991) and Carr (2002):

$$k = k_w + 0.0088 \times C + 0.054 \times C^{0.66} \quad (3)$$

where k_w is the attenuation coefficient of pure sea water (equal to 0.04).

P(z) is expressed as carbon production in mgC m^{-3} h^{-1}. In the southern Benguela region, α^B = 0.0193 and P^B_m = 3.61 are typical values (Mitchell-Innes 2000), obtained by averaging all measured values. Despite their large variability in space and time in upwelling systems, these values are close to those reported in Chilean upwelling areas (α^B = 0.021 and P^B_m =2.84, Montecino et al. 2004). Although P^B_m is known to represent physiologically related variability and generally has a positive relationship with temperature, no data are currently available to explore this variability at spatial and temporal scales compatible with our regional approach. Furthermore, the value of P^B_m used here is calculated for an average SST of 15°C, which is also the average seasonal SST in most of our area of interest.

RESULTS

Characterising vertical profile shapes

The SOM map of 15 characteristic chl *a* profiles obtained from 2498 data profiles is shown in Fig. 2. Ordering of the map is based on the SOM multivariate

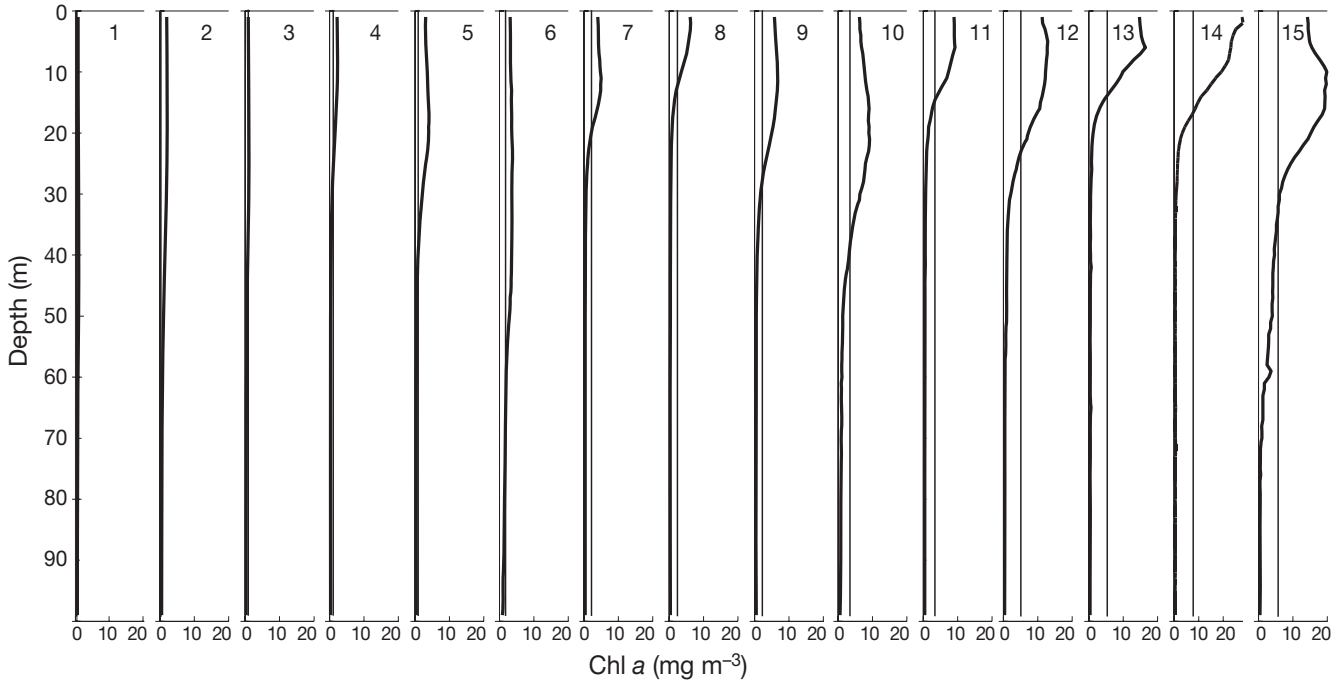

Fig. 2. Self-organic maps (SOM) patterns: the output map of the 15 × 1 SOM of vertical chl *a* profiles using 2498 profiles as input. The SOM output map of characteristic profiles is numbered from 1 to 15

analysis over all depths. This produces a matrix of characteristic depth profiles and a map in which the characteristic profiles are ordered. The characteristic chl *a* profiles represent common patterns in the data. The procedure has arranged the profiles according to common patterns, ranging from Profile 1 with little vertical structure, low surface chl *a* and low integrated chl *a*, to Profile 15 with clear subsurface peaks and high surface and water-column integrated chl *a*, with a gradation in between. Some of the characteristic profiles have highest chl *a* values near the surface, while others have subsurface peaks.

Table 1 gives the surface and water-column integrated chl *a* values of each of the characteristic profiles identified by the SOM. Because the actual chl *a* profiles were used in this analysis, it is of interest to assess how closely a Gaussian distribution fits these characteristic profiles, which are obtained without any assumptions about profile shape. Visually, the profile shapes resemble the Gaussian distribution quite closely. Generalised chl *a* profiles identified by the SOM were compared with the standard shifted Gaussian model (not shown). Table 1 also shows the goodness of fit (r^2) to a shifted Gaussian curve. These values have only been calculated down to 50 m because there is little variation in the profiles below this depth. The shifted Gaussian curve represents all 15 characteristic profiles reasonably well, although Profiles 1 and 6 show some deviation from this shape

Relationships of profiles to surface variables

The GAM for predicting the 15 characteristic profile shapes from the suite of surface variables is shown in Fig. 3a. The GAM explains 88.1% of the variability in profile shape. Each plot illustrates the non-linear relationship between the response (profile number) and each predictor (adjusted for all other predictors in the model). The *y*-axis is a relative scale, and a positive *y*-value indicates a positive effect on the response (see Fig. 3 caption). Note that none of the relationships in Fig. 3a are linear, supporting the use of a GAM.

Surface chl *a* is by far the best predictor of profile number (note the range of the *y*-axis is much larger than for other variables) and shows a generally increasing relationship between the profile map (ordered by the SOM) and surface chl *a*. Profile number is also related to season, with significantly higher values in summer than any other season, and the profile number is higher in spring than in autumn or winter. Profile number also varies regionally, with the west coast having significantly higher profile numbers than the Agulhas Bank areas. In terms of temperature, highest profile numbers are found at intermediate SST (13 to 16°C), this range being typical of warming upwelled water, with lower profile numbers evident in cool recently upwelled water and in warmer offshore water. Profile number is not substantially influenced by depth of water column (a surrogate for distance offshore), as the wide confidence limits suggest a weak relationship.

The result of the GLM parameterised by inspection of the GAM is shown in Fig. 3b. We parameterised the non-linear continuous variables in Fig. 3a using piecewise linear regressions, with a breakpoint at 7 mg m^{-3} for surface chl *a*, and a breakpoint at 15°C for SST (Fig. 3b). Four of the predictors are significant and are retained in the GLM (see ANOVA table for the GLM in Table 2), as the fifth (Depth) was not significant and was dropped from the predictive model. The total variance explained by the GLM is 87.4%. Surface chl *a* concentration (73.3%) is the most important predictor of profile number, followed by area (7.1%), season (6.8%) and SST (0.2%). The GLM equation to predict profile number is given in Table 3.

Table 2. ANOVA table for the generalised linear model predicting the characteristic profile number (1 to 15) from the SOM in Fig. 2 from 4 predictors. The variance explained (r^2) by the model is 87.4%. The predictor, water column depth, was not significant and was removed from the model. Sums of squares (deviance), degrees of freedom (df), *F*-ratio, and significance level (p) are given

Effect	Deviance	df	*F*	p
Area	2053.34	2	702.65	0.0000
Chl term	21 093.70	2	7218.27	0.0000
SST term	42.69	2	14.608	0.0000005
Total	28 783.16	2497		

Table 1. Characteristics of the 15 profiles from the SOM in Fig. 2 including: surface value, integrated value, and goodness of fit (r^2) to a shifted Gaussian curve (Platt & Sathyendranath 1988, Longhurst et al. 1995, Sathyendranath et al. 1995) down to 50 m depth

Profile number	1	2	3	4	5	6	7	8	9	10	11	12	13	14	15
Surface value	0.38	1.94	0.91	2.16	3.1	3.11	4.02	6.02	5.82	6.18	8.89	11.23	14.72	27.68	14.24
Integrated chl *a*	37	121	61	73	139	253	121	96	196	344	161	308	222	382	589
r^2 Gaussian	0.82	0.99	0.97	1.00	0.98	0.82	0.99	1.00	1.00	0.99	1.00	1.00	1.00	1.00	0.96

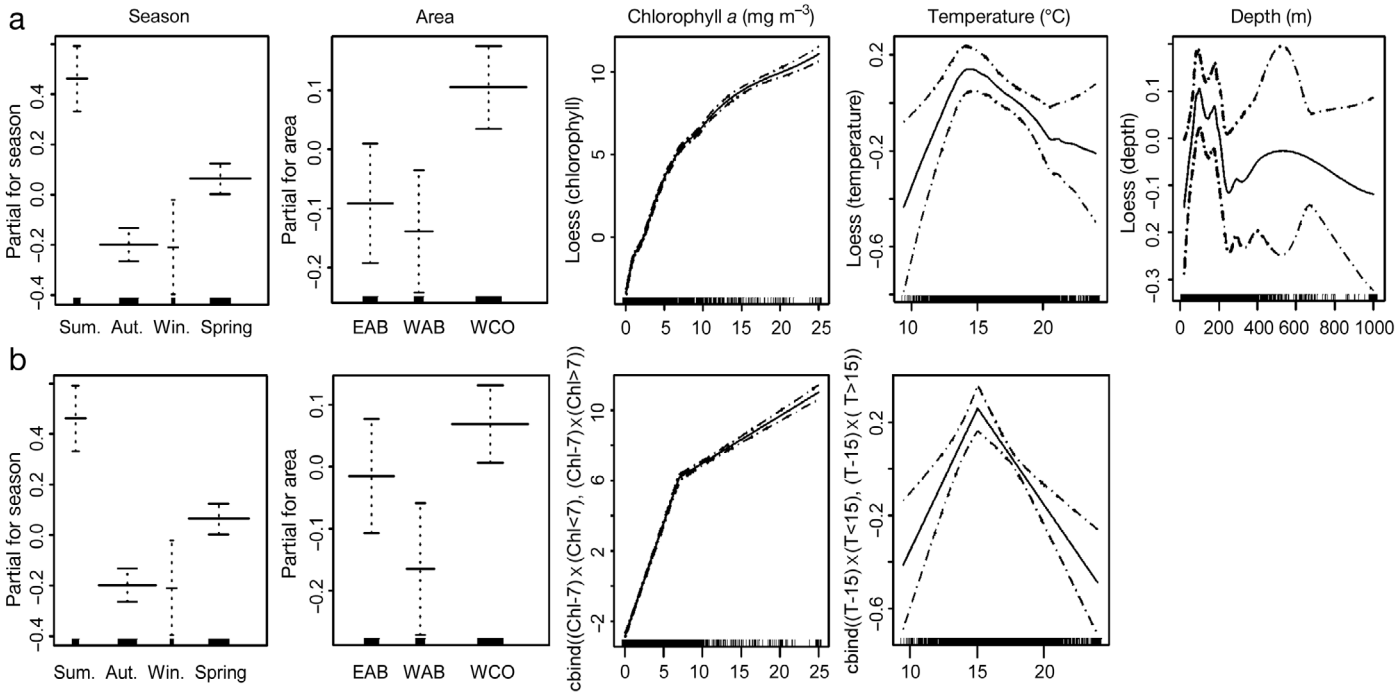

Fig. 3. Generalised models relating vertical profile shape to a suite of predictors: (a) The generalised additive model (GAM) predicts the characteristic profile number (1 to 15) from the SOM in Fig. 2. The *y*-axes are transformed relative to the predictor variables on the *x*-axes (Hastie & Tibshirani 1990). The *y*-axis is a relative scale, so that a *y*-value of zero is the mean effect of the adjusted environmental variable on the response, a positive *y*-value indicates a positive effect on the response, and a negative *y*-value a negative effect on the response. The mean and 95% confidence intervals are shown in each plot, and a rug plot indicating the distribution of raw data is included on the *x*-axis. Predictors used were season, area, surface chl *a* concentration, SST and water column depth. (b) The corresponding generalised linear model (GLM) using a piecewise linear regression for chl *a* and temperature (see Table 3 for equation details). Water column depth was not significant and, thus, not included in the GLM model. EAB: Eastern Agulhas Bank; WAB: Western Agulhas Bank; WCO: West Coast; cbind: breakpoint between 2 straight lines

Distribution of characteristic profiles

Our area of study was initially subdivided into 5 sub-areas based on the spatial and seasonal variability of primary production and on local hydrography. For simplicity of presentation, these were later reduced to produce only 3 sub-areas (numbered in Fig. 1). Note that Areas 1 and 2 are different from sub-areas used for modelling shipboard profiles (west coast and western Agulhas Bank, see Fig. 1). The Namaqua cell is included in Area 1, and the St. Helena Bay (32° S) and Cape Peninsula (33 to 34° S) cells plus the western Agulhas Bank (from Cape Point to Cape Agulhas, 18.5 to 20° E) are all represented in Area 2. The south coast includes the central and eastern Agulhas Bank (up to 29° E) and forms Area 3. Fig. 4 shows the distribution of the 15 characteristic chl *a* profiles for each pixel by area and season over the 6 yr period of satellite observations, as modelled by the GLM. Profiles have been pooled into 4 groups for simplicity, with Profiles 1 to 4 having the lowest integrated chl *a* and 13 to 15 the highest.

Seasonal changes in chlorophyll and primary production

We used this predictive relationship based on remotely sensed SST and surface chl *a* to predict the profile shape at any location and time. Surface chl *a* biomass is shown in Figs. 5a & 6a; this was used to calculate seasonal maps of integrated chl *a* (Figs. 5b & 6b) using the generalised model and primary production (Figs. 5c & 6c) using the bio-optical model.

In terms of surface chl *a*, maximum densities (>20 mg m^{-3}) and greatest offshore extent (200 km) are found on the west coast from St. Helena Bay northwards (29 to 33° S) from austral spring to autumn (Fig. 5a). Integrated chl *a* (Figs. 5b & 6b) attains its greatest offshore extent (150 to 200 km) on the west coast in spring and summer with a local maximum of >400 mg m^{-2} in St. Helena Bay (Fig. 5b), while the maximum integrated chl *a* appears in spring farther north on the west coast. Integrated chl *a* peaks on the south coast during autumn (Fig. 6b) corresponding to surface chl *a* of >8 mg m^{-3} and integrated values of >200 mg m^{-2}. Maximum rates of primary production

Table 3. Equation of the generalised linear model (GLM) for predicting characteristic profile number (1 to 15) from the SOM in Fig. 2. Predictors used were season, area (EAB, WAB, WCO; see Fig. 1), surface chl *a* concentration and sea surface temperature (SST)

$$Y = 10.3702 + \begin{cases} 0, & \text{if season = Summer} \\ -0.2816, & \text{if season = Autumn} \\ -0.0948, & \text{if season = Winter} \\ 0.0156, & \text{if season = Spring} \end{cases} + \begin{cases} 0, & \text{if region = EAB} \\ -0.0749, & \text{if region = WAB} \\ -0.0530, & \text{if region = WCO} \end{cases} + \begin{cases} 1.2876 \times (\text{chl}-7), & \text{if chl} < 7 \\ 0.2688 \times (\text{chl}-7), & \text{if chl} \geq 7 \end{cases} + \begin{cases} 0.1203, & \text{if SST} < 15 \\ -0.0830, & \text{if SST} \geq 15 \end{cases}$$

seasonally reach 5 to 6 g C m^{-2} d^{-1} on the west coast (Fig. 5c). Primary production is higher from Cape Agulhas all the way up the west coast in spring and summer, reflecting the higher PAR. Similar to the surface and integrated chl *a*, the centre of maximum primary production is farther north on the west coast (north of Hondeklip Bay) during spring. Highest average primary production (ca. 2.5 g C m^{-2} d^{-1}) on the Agulhas Bank is found on the far eastern Bank (23 to 27° E) in summer (Fig. 6c). The large distinct autumn feature on the eastern Bank between 21 and 22° E is clearly evident in the surface and integrated chl *a* maps in autumn, but only leads to slightly faster primary production rates than in summer.

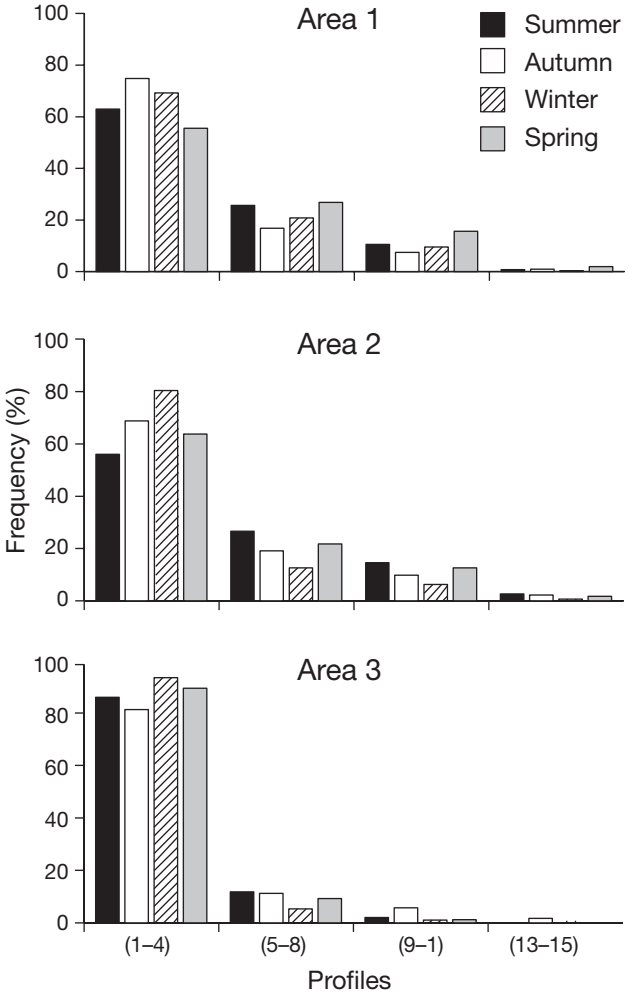

Fig. 4. Distribution of 15 characteristic profiles (depicted in Fig. 2) as modelled for each pixel, classified by area and season over the 6 yr period of satellite observations. Profiles range from 1 (low integrated chl *a*) to 15 (high chl *a*) for the 3 areas defined in Fig. 1. Austral seasons arranged from summer (January–March) to spring (October–December)

Maps of surface and integrated chl *a* are most different in areas where subsurface peaks are more common. For example, elevated surface chl *a* values on the Eastern Agulhas Bank (ca. 25 to 26° E) correspond to relatively moderate values of integrated chl *a*. In terms of primary production, the same area shows even greater differences, mainly in autumn and winter when light is limiting.

Monthly averages of surface chl *a*, integrated chl *a*, primary production and PAR were computed for each of our defined areas (Fig. 7). Areas 1 and 2 have similar seasonal ranges in surface chl *a*, integrated chl *a* and primary production. Values for primary production in Areas 1 and 2 range from 1 to 2 g C m^{-2} d^{-1} throughout the year, whereas that in Area 3 ranges from 0.75 to 1.5 g C m^{-2} d^{-1}.

In terms of seasonal variation, surface chl *a* concentration in Areas 1 and 3 has less seasonality than Area 2 (coefficients of variation [CV] of 20 and 22%, respectively, against 30%). However, vertically integrated chl *a* (Fig. 7a) is less variable seasonally in all areas (CVs of 12, 9 and 16%, respectively, for Areas 1, 3 and 2). The seasonality of the primary production (Fig. 7b) is again more pronounced (average CV of 29%) than that of the surface and integrated chl *a* for all areas, reflecting the seasonality of PAR.

Overall changes in chlorophyll and primary production

A space-time diagram (Hovmoller plot) summarises the spatio-temporal variability of primary production in the region (Fig. 8) by averaging the production between the coast and the 0.5 mg m^{-3} offshore limit of surface chl *a* and over the depth dimension down to the 1% light level. This diagram summarises the primary production estimated for every pixel of coastline and for every month, highlighting the inter-annual,

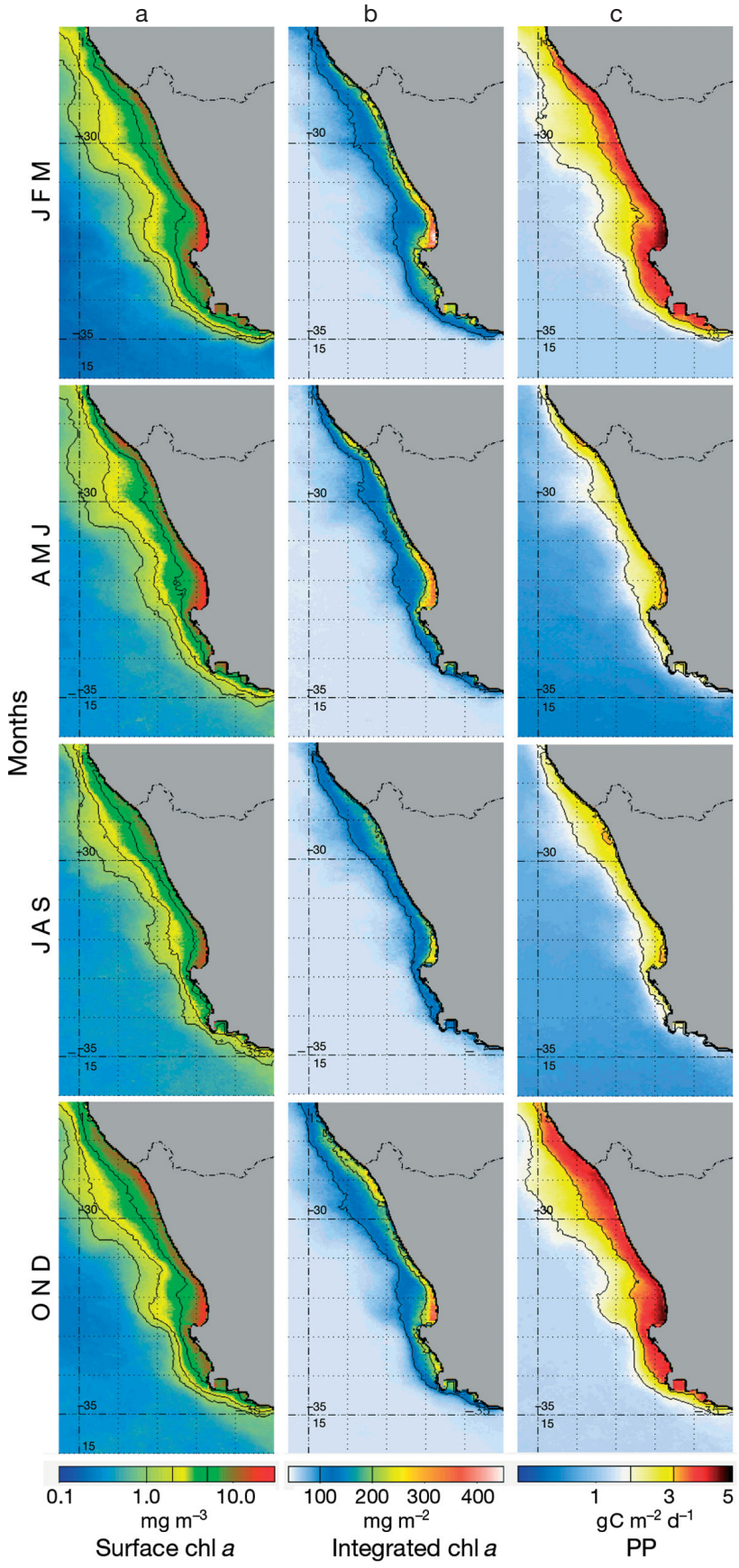

Fig. 5. West coast (Africa) maps of seasonal averages for (a) SeaWiFS remotely sensed surface chl *a*, (b) integrated chl *a* biomass computed from the generalised linear model and (c) primary production (PP) calculated from the integrated chl *a* and a light algorithm. Coordinates are latitude (°S) and longitude (°E)

seasonal and latitudinal variations in primary production.

The primary production shows strong seasonality, with clear winter minima (between June and July), mainly driven by sunlight. The latitudinal variability is high and is associated with the main upwelling cells. The west coast area is characterised by consistently fast production rates around 28 to 29° S (Orange River) and 32 to 34° S (St. Helena Bay to Cape Peninsula), with monthly average maxima between 4 and 6 g C m^{-2} d^{-1}. A similar production level is observed between the Cape Peninsula and 20° E (Cape Agulhas), an area of strong seasonality, whereas the rest of the south coast appears to be much less productive, except between 26 and 28° E (around Port Elizabeth) and much more episodically between 22 and 26° E during summer (maxima around 3 gC m^{-2} d^{-1}).

Fig. 9 shows the inter-annual dynamics of the primary production of the 3 areas defined in Fig. 8 (see Fig. 1 for location). No trend is visible and no particular year stands out dramatically above or below the average. Some particularly high values are observed in summer in 1998 (Area 1, ca. 2.5 gC m^{-2} d^{-1}) and in 2000 (Area 2, ca. 2.2 gC m^{-2} d^{-1}), and some low values in 2001 and 2002. It is interesting to note that even at the monthly time step of the study, at least 2 peaks of production generally occur in summer, showing the dynamic nature of the upwelling. There are also marked changes in the shape of this seasonal cycle each year. For example, Area 3 shows peaks early in the upwelling season in 1997–98, 1998–99, 2001–02, but peaks later in the season in 1999–2000, 2000–01, and 2002–03.

Despite these observations, the inter-annual CV is particularly low and stable across seasons and areas (CV = 5.5%

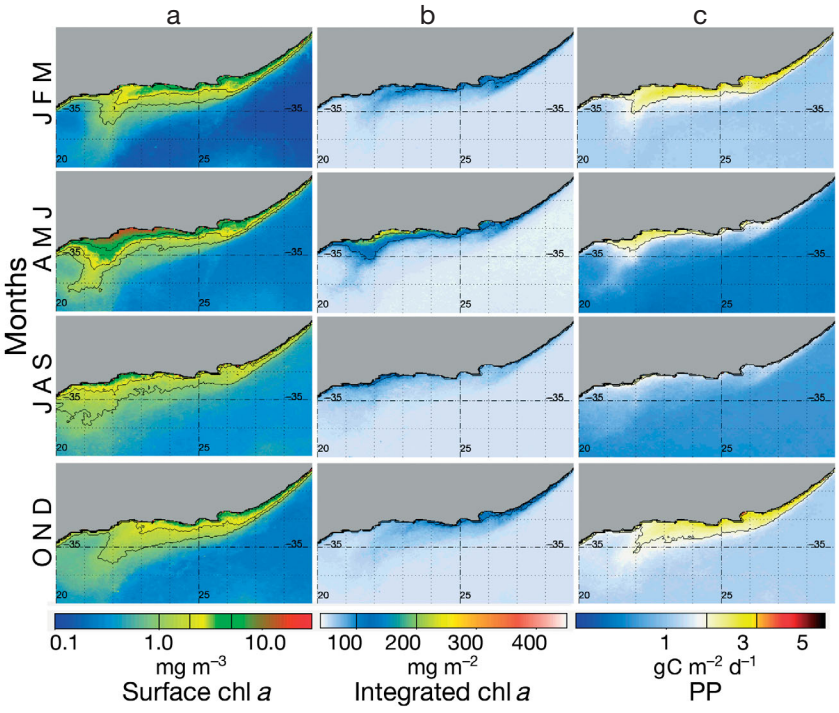

Fig. 6. South coast (Africa) maps of seasonal averages for (a) SeaWiFS remotely sensed surface chl *a*, (b) integrated chl *a* biomass computed from the generalised linear model and (c) primary production calculated from the integrated chl *a* and a light algorithm. Coordinates are latitude (°S) and longitude (°E)

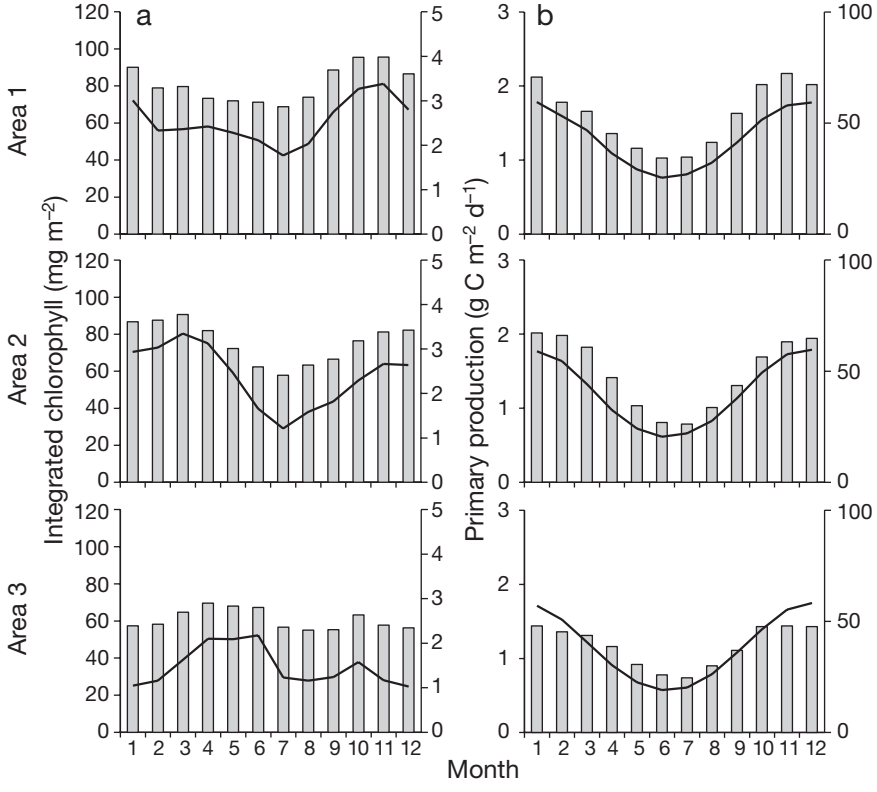

Fig. 7. Monthly averages of (a) integrated chl *a* (bars) and surface chl *a* (line), and (b) primary production (bars) and PAR (lines) for each of the 3 areas defined in Fig. 1

on average). All partial inter-annual CVs (by areas and by seasons) range from 3.3 to 7.8%.

Total primary production and sensitivity tests

The annual primary production averaged over the 6 yr period of study is shown in Fig. 10. Highest values are inshore on the west coast, delimited by the 3 gC m^{-2} d^{-1} contour. The contours for 2 and 1 gC m^{-2} d^{-1} are also given. Table 4 summarises values of surface chl *a*, integrated chl *a* biomass and primary production for each of the 3 areas. Areas 1 and 2 appear to be very similar in terms of surface chl *a* (2.6 to 2.7 mg m^{-3}) and very close in terms of biomass (78 and 76 mg chl *a* m^{-2}, respectively) and primary production (1.6 gC m^{-2} d^{-1} for both areas). Area 3 shows lower average values of surface chl *a* (1.4 mg m^{-3}), but comparatively high values of production (1.2 gC m^{-2} d^{-1}). Total primary production in all 3 areas reaches 156 million tC yr^{-1}.

Several tests were performed to evaluate the sensitivity of production values to input variables of the model: surface chl *a*, PAR and the photosynthesis parameters, α^B (alpha) and P^B_m (hereafter given as P_{max}), as well as the potential sensitivity of P_{max} to temperature (not included in the model). The tests involved applying a range of variability (–50%, +50%) to the 4 main input variables, with the exception of PAR (–30%, +30%) because the observed variability of PAR is lower and less subject to variability at the monthly scale we used.

Results are expressed in terms of a sensitivity factor, defined as the ratio of the observed variation of the output variable (primary production) to the variation applied to the tested input variable. Thus, a sensitivity factor of +0.5 indicates that we observed a positive increase of production of only 50% corresponding to an increase of 100% of the input variable.

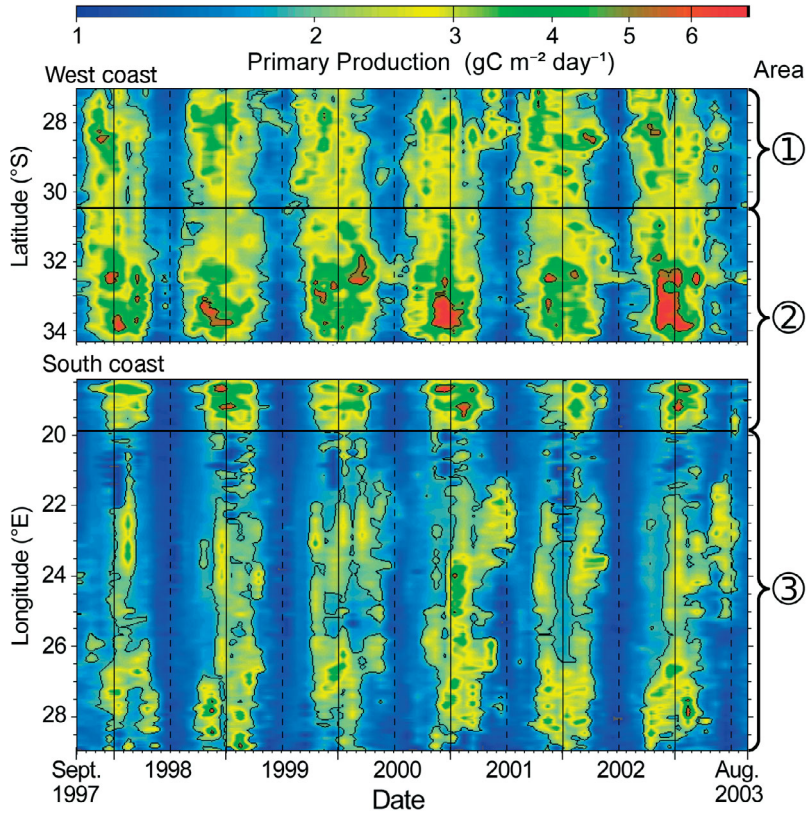

Fig. 8. Hovmoller plot of primary production on the west and south coasts of southern South Africa over the 6 yr period of satellite observations. The geographic areas numbered on the right are those of Fig. 1. Values are averaged spatially between the coast and the 0.5 mg m^{-3} offshore limit of surface chl *a*. Values of 3 and 6 mg C m^{-2} d^{-1} are contoured

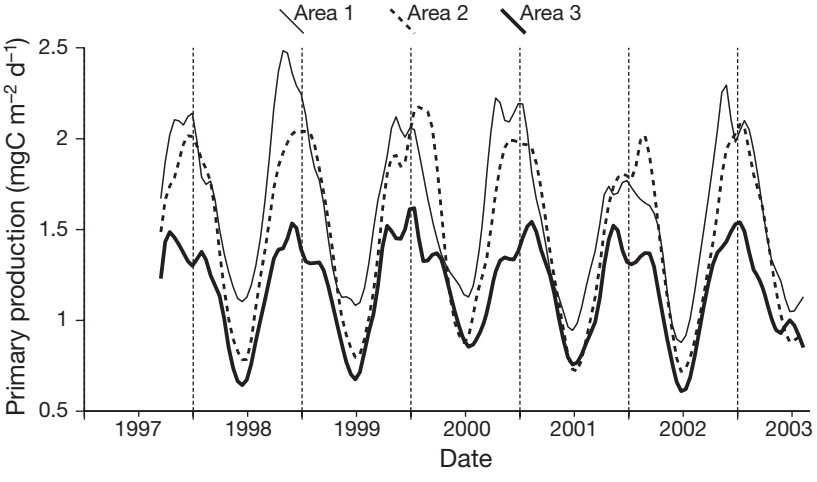

Fig. 9. Smoothed time series from 1997 to 2003 of average monthly primary production in the southern Benguela and Agulhas Bank systems for each of the 3 areas defined in Figs. 1 & 8

Fig. 11 shows that the sensitivity of modelled primary production varies among the *P-E* variables by a factor of >3, from 0.4 to 1.3, being the least sensitive to surface chl *a* and most sensitive to alpha. Surface chl *a* and P_{max} have moderate and similar sensitivity factors, respectively 0.34 and 0.43. The importance of PAR is significantly greater (0.58), while alpha, the initial slope of the photosynthesis function, gives a high average sensitivity factor of 1.15. Sensitivity decreases in a somewhat linear manner for all 4 variables as they are changed from −50 to +50%. These trends can be explained by the exponential attenuation of light through the water column; clearly attenuation also increases with the average algal concentration. Interaction effects were also tested (results not shown) and indicate only a slight reduction compared with the sum of the individual effects, notably between surface chl *a* and PAR (−2 to +2%) and slightly more between alpha and P_{max} (−7 to +7%), with a tendency to stabilize the output value. The most important conclusion is that all effects are globally cumulative.

Finally, we tested the potential influence of SST on P_{max}, by simulating incorporation of the classic relationship of Eppley (1972):

$$P_{max}(T) = 1.065^{(T-20°)} \times P_{max}(20°) \quad (4)$$

(where T is temperature) which is included in several bio-optical models (e.g. Morel 1991), keeping in mind the lack of consensus on the effect of temperature on primary production. In our area of interest, the upwelling is maximum during summer, so that the seasonal amplitude of the SST is reduced (Demarcq et al. 2003) and varies from 12 to 18°C. Following the Eppley (1972) relationship, the effect on P_{max} ranges from −13 to +15%, corresponding to an effect on primary production ranging from −6 to +6% (from the previous sensitivity of P_{max} itself). Consequently, accounting for SST would moderately increase the seasonal amplitude of our modelled primary production with a slight increase in summer values and a slight decrease in winter. No significant bias is expected since the parameters of the *P-E* function used in the model are calculated from *in situ* measurements collected for an

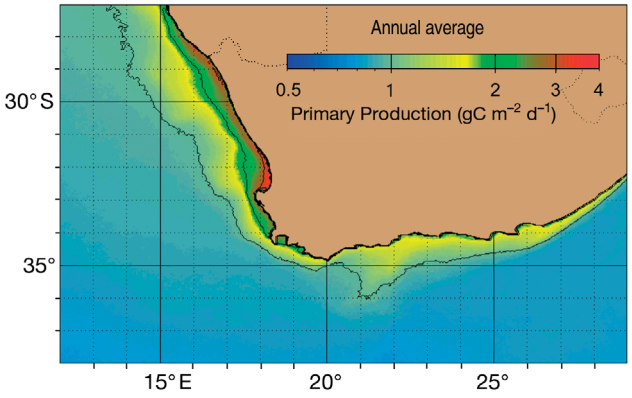

Fig. 10. Annual average primary production from 1997 to 2003. Values of 1, 2 and 3 mg C m^{-2} d^{-1} are contoured

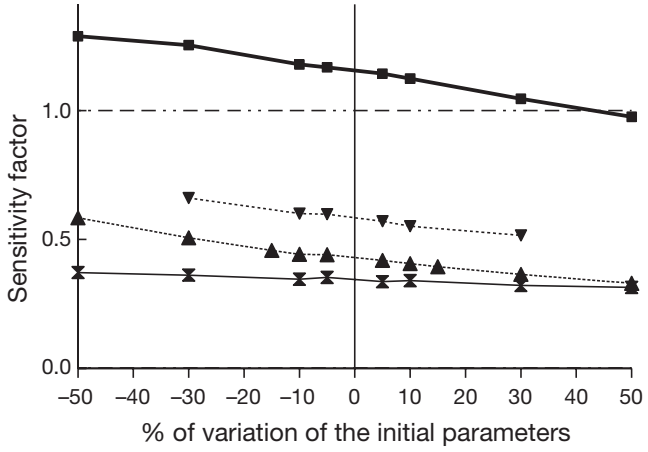

Fig. 11. Sensitivity of primary production to the input parameters of the primary production model (⧗: surface chl *a*, ▼: PAR, ■: alpha, ▲: P_{max})

average SST of 15°C (Mitchell-Innes 2000), which is also the average SST for our area of interest. A future improvement would be to use a full vertical profile of temperature instead of the SST alone to test more accurately the influence of the temperature on P_{max} at each depth level.

DISCUSSION

The approach outlined here, of applying a simple primary production model to identify probable profiles from remotely sensed data, has produced robust estimates of primary production in the Benguela and Agulhas Bank systems, especially in terms of capturing its spatial and temporal variability. Previous estimates have been based on limited sets of *in situ* data, with little information on the spatial and vertical distribution of the biomass and even less on its temporal variability, with the exception of preliminary studies using remote sensing data sets based on chl *a* concentrations (De Villiers 1998, Demarcq et al. 2003). Our method combines results from nearly 2500 *in situ* profiles with monthly satellite images, allowing us to capture the spatio-temporal variability in upwelling. This simple approach can also be applied easily to other regions of the world, provided that there are sufficient vertical chl *a* profiles to develop models linking surface to *in situ* measurements. Such profiles are becoming increasingly available from national oceanographic data centres as chlorophyll sensors are added to floats, gliders, and yo-yo buoys as part of the Global Ocean Observing System (GOOS).

The procedure of estimating *in situ* chl *a* profiles is consistent with the growing need for data assimilation techniques to integrate measurements and knowledge of ecological processes on large spatio-temporal scales. This is particularly the case in marine science where sampling is generally coarse compared with the dynamic nature of the environment, even at the primary production level. Physical and coupled biogeochemical models provide useful information from a dynamic point of view, but only make use of *in situ* data for calibrating internal processes or for model validation. At the regional scale, the use of relatively simple generic statistical approaches can distil information from large *in situ* data sets, which is particularly useful for integrating the large volumes of ocean surface data acquired from space.

Table 4. Annual average surface chl *a*, integrated biomass and primary production by areas and overall temporal variability computed from monthly values. Also shown are seasonal primary production values. (–): no data available

Parameter	Unit	Total	SD	CV (%)	Area 1	Area 2	Area 3
Surface chl *a*	mg chl m^{-3}	2.2	0.52	24	2.6	2.7	1.4
Integrated chl *a*	mg chl m^{-2}	69.8	7.04	10	77.7	76.1	58.9
Primary production	g C m^{-2} d^{-1}	1.4	0.37	26	1.6	1.6	1.2
Summer	g C m^{-2} d^{-1}	_	_	_	1.9	2.0	1.4
Autumn	g C m^{-2} d^{-1}	_	_	_	1.2	1.2	1.0
Winter	g C m^{-2} d^{-1}	_	_	_	1.3	1.1	0.9
Spring	g C m^{-2} d^{-1}	_	_	_	2.1	1.9	1.4
Area	km^2 × 1000	302	_	_	83	99	119
Annual production	million t C yr^{-1}	156	0.06	0.04	49	56	51

Possible sources of error and model sensitivity

We have chosen a primary production model that makes maximum use of the information about the vertical dimension for biomass and light propagation, although the spectral influence of the light attenuation is not resolved in the model. The consequence is generally a slight under-estimation of the values of primary production corresponding to surface chl *a* values of <2 mg m^{-3}. No data on the seasonal or spatial dependence of the parameters of the *P-E* relationship in the region were available for use in the model. In addition, our production estimates may be lower than *in situ* measurements because it is not easy to consider photo-adaptation of phytoplankton at this scale.

The tests on the model sensitivity supply useful information on the most important variables to be considered in the production model. Behrenfeld & Falkowski (1997) state that '85% of the variability in primary production can be attributed to changes in depth-integrated biomass and less than 15% to PAR.' This does not consider the uncertainty in variability of the photosynthesis parameters, but it does show the importance of considering the vertical structure of the biomass, rather than making an indirect estimate from the depth of the mixed layer, as other models do. The recent comparison of global estimates of primary production from the third generation algorithm of primary production (Carr et al. 2006) clearly shows that most models (none of which use a global coverage of chl *a* profiles) generate a sensitivity factor of 0.75, which is by far the most sensitive input variable of all the global models tested. This value is approximately more than twice the sensitivity factor we found for the surface chl *a* in our model. Also, chl *a* is the variable to which our model is the least sensitive.

Nevertheless, it is clear that photosynthesis-related parameters remain among the most sensitive in the model, particularly alpha, the slope of the *P-E* function, but also P_{max}, which is less sensitive, but whose natural range of variation is probably higher. Its variant P^{B}_{opt} (optimum photosynthetic biomass), is believed to account not only for light, but for the photo-adaptive yield, which itself depends on numerous *in situ* conditions, such as temperature, nutrient concentration and the functional group of phytoplankton, a set of variables for which little is known. As stated by Carr et al. (2006), 'The large divergence in response to SST perturbations illustrates the need to improve our understanding, and ability to model, the effect of temperature on photosynthesis.' From the same study, it appears that along with a better formulation of the quantum yield and the light field, more data are generally needed on the vertical distribution of chl *a*. In particular, 'assumptions of steady state and balanced growth inherent to bio-optical primary production models cannot reproduce the unsteady disturbed environment of cells in the ocean.'

Spatial and temporal variability

Platt & Sathyendranath (1988) have shown that a biogeographical approach including water column considerations is strongly recommended when applying primary production algorithms on a large scale. The spatial and temporal variation of surface chl *a*, integrated chl *a* and primary production estimates produced in this study are a consequence of the large-scale meteorological forcing of the area. The major up-welling cells of Namaqua, St. Helena Bay and the Cape Peninsula are clearly identified as areas of enhanced chl *a* biomass and primary productivity. Upwelling occurs during spring and summer in these seasonal cells of the southern Benguela, coinciding with the times when the trade winds are farthest south and wind in the region is strongest (Parrish et al. 1983, Shannon 1985, Hardman-Mountford et al. 2003). This movement of the trade winds leads to strong seasonality in integrated chl *a* and primary productivity off the west coast of southern South Africa (Areas 1 and 2), reaching a maximum in spring and summer (Fig. 5). By contrast, the relatively stable Agulhas Bank (Area 3) has consistent values of integrated chl *a* and primary productivity throughout the year, with only a moderate dip in autumn and winter (Fig. 6).

This seasonal movement of the wind field also affects the shape of chl *a* profiles. Areas 1 and 2 on the west coast have shallower peaks (i.e. profile number > 5) in spring and summer (Fig. 4). These areas have high frequencies of the low biomass profiles in autumn and winter. The more stratified Agulhas Bank area has a high frequency of pixels (>80%) with chl *a* profiles that have low and uniform biomass (Area 3 in Fig. 4), a consequence of the reduced southerly winds in this area. During winter, the dominant winds over the Agulhas Bank are mid-latitude westerlies (Boyd & Shillington 1994), which result in deep mixing, and at this time profiles with low integrated chl *a* are more common than in other seasons.

Estimates of primary production

Our estimates are similar to, but slightly lower than, estimates made in earlier studies of phytoplankton productivity off the southwest of Africa (Table 5). For the area from 29° S to Cape Point (ca. 34° S), the total primary production is 70 million t C yr^{-1}, which is slightly lower than previous values of 76 million t C yr^{-1}

Table 5. Comparisons of primary production, surface of productive areas, total biomass (*B*), annual primary production (*P*) and *P*:*B* ratio, averaged over the southern Benguela from 29° S to Cape Point (ca. 34° S)

Surface chl *a* (mg chl m^{-3})	Primary production (g C m^{-2} d^{-1})	Productive area ($km^2 \times 1000$)	Total biomass (million t C)	Annual primary production (million t C yr^{-1})	*P*:*B* (d^{-1})	Data source
2.9	1.6	119	0.94	70	0.21	Present study
2.2	2.0	104	0.67	76	0.31	Brown et al. (1991)
2–3	2.6	95	_	100	_	Carr (2002)

(Brown et al. 1991) and 100 million t C yr^{-1} (Carr 2002). Our annual average estimate for primary productivity for the central and eastern Agulhas area (Area 3) of 1.2 gC m^{-2} d^{-1} (Table 4) is also lower than the few observed values for this area that have been collected with a seasonal bias (Probyn et al. 1994).

The first detailed time series of estimated primary production along the South African coastline provided here can be used to tease apart contributions of primary production, transport and retention to the recruitment of small pelagic fish (Bakun 1996). For example, there has been no increase in primary production over the period of this study, but there has been an increase in the biomass of pelagic fish (van der Lingen et al. 2006). The small inter-annual range in primary production and its lack of trend would not support the increased production of sardine and anchovy over this period if the fishery were driven by bottom-up processes alone (van der Lingen et al. 2006). This is especially the case during the summer of 2001–2002 when there was lower than average primary production (Fig. 9), but record recruitment of sardine. Thus, it appears that primary production may not be the most important limiting factor for these stocks in the southern Benguela region at present levels of exploitation, and physical factors such as advection and retention may be important (Bakun 1993, Lett et al. 2006).

In conclusion, this paper provides a novel method for combining the advantages of frequent spatial coverage of the ocean surface from satellites with sparser archives of vertical chl *a* profiles. This has been illustrated by data from the southern Benguela upwelling region and the seasonally stratified Agulhas Bank. We were able to simplify the inherently complex 3-dimensional spatial variability of primary production by integrating both through depth (1% light level) and across an adequate boundary offshore (the 0.5 mg m^{-3} limit of surface chl *a*) along the coast. This integration strongly reduces the uncertainty of the modelling regarding the influence of surface chl *a* values. We provide the most detailed vertically integrated estimates to date of chl *a* and primary production in both time (monthly over 6 yr) and space (ca. 25 km^2 pixels). Our work estimates the total primary production in the Benguela system together with the Agulhas Bank at ca. 156 million t C yr^{-1}. This estimate should be of use to existing and future mass balance and simulation models within the region (e.g. those by Shannon et al. 2004a,b), since it covers the range of migration of many fish species. We suggest that this approach could be applied in different biogeochemical provinces of the world's oceans, given appropriate data for each region in accord with Platt & Sathyendranath (1988) who argued in favour of a biogeographical approach with water column considerations when applying primary production algorithms at a large scale. With the imperative to adopt an ecosystem approach to fisheries by 2010 (United Nations 2002), we also hope that the time series of primary productivity estimates provided here will help underpin ecosystem models that can be used to support fisheries management in the future.

Acknowledgements. We thank the SeaWiFS Science Project for providing the SeaWiFS Level 2 data set, including chl *a* and PAR data. We also thank the Chief Director, Research and Development of Marine and Coastal Management, Department of Environmental Affairs and Tourism, South Africa, for permission to use shipboard chl *a* profile data, as well as 3 anonymous referees for their valuable comments that helped us improve the manuscript. We thank the Marine Biological Association of the UK for a Ray Lankester Fellowship that enabled J.G.F. to devote time to this study. This is a contribution to the ECO-UP programme, which involves the IRD (Institut de Recherche pour le Développement), Marine and Coastal Management, and the University of Cape Town, among other partners.

LITERATURE CITED

Antoine D, André JM, Morel A (1996) Oceanic primary production 2. Estimation at global scale from satellite (coastal zone color scanner) chlorophyll. Glob Biogeochem Cycles 10:57–69

Baith K, Lindsay R, Fu G, McClain CR (2001) SeaDAS: data analysis system developed for ocean color satellite sensors. EOS Trans Am Geophys Union 82:202–205

Bakun A (1993) The California Current, Benguela Current, and southwestern Atlantic Shelf ecosystems: a comparative approach to identifying factors regulating biomass yields. In: Sherman K, Alexander LM, Gold BD (eds) Large marine ecosystems: stress, mitigation and sustainability. Am Assoc Adv Sci Press, Washington, DC, p 199–221

Bakun A (1996) Patterns in the ocean: ocean processes and marine population dynamics. University of California Sea Grant, San Diego, CA

Behrenfeld MJ, Falkowski PG (1997) Photosynthetic rates derived from satellite-based chlorophyll concentration. Limnol Oceanogr 42:1–20

Boyd A, Shillington SA (1994) The Agulhas Bank: a review of the physical processes. S Afr J Sci 90:114–122.

Brown PC, Painting SJ, Cochrane KL (1991) Estimates of phytoplankton and bacterial biomass and production in the northern and southern Benguela ecosystems. S Afr J Mar Sci 11:537–564

Campbell J, Antoine D, Armstrong R, Arrigo K and others (2002) Comparison of algorithms for estimating ocean primary production from surface chlorophyll, temperature, and irradiance. Global Biogeochem Cycles 16(3)1035

Carr ME (2002) Estimation of potential productivity in Eastern Boundary Currents using remote sensing. Deep-Sea Res II 49:59–80

Carr ME, Friedrichs MAM, Schmeltz M, Aita MN and others (2006): A comparison of global estimates of marine primary production from ocean color. Deep-Sea Res II 53:741–770

Cullen JJ (1982) The deep chlorophyll maximum: comparing vertical profiles of chlorophyll *a*. Can J Fish Aquat Sci 39: 791–803

Cullen JJ, Lewis MR (1995) Biological processes and optical measurements near the sea surface: some issues relevant to remote sensing. J Geophys Res 100:13255–13266

Demarcq H, Citeau J (1995) Sea surface temperature retrieval in tropical area with METEOSAT: the case of the Senegalese coastal upwelling. Int J Remote Sens 16:1371–1395

Demarcq H, Barlow R, Shillington FA (2003) Climatology and variability of sea surface temperature and surface chlorophyll in the Benguela and Agulhas ecosystems as observed by satellite imagery. Afr J Mar Sci 25:363–372

De Villiers S (1998) Seasonal and inter-annual variability in phytoplankton biomass on the southern African continental shelf: evidence from satellite-derived pigment concentrations. In: Pillar SC, Moloney CL, Payne AIL, Shillington FA (eds) Benguela dynamics. S Afr J Mar Sci 19:169–179

Eppley RW (1972) Temperature and phytoplankton growth in the sea. Fish Bull 70:1063–1085

FAO Marine Resources Service, Fishery Resources Division (2005). Review of the state of world marine fishery resources. FAO Fish Tech Pap No. 457, Rome

Frouin R, Franz B, Wang M (2003) Algorithm to estimate PAR from SeaWiFS data. Version 1.2 – documentation. NASA Tech Memo 206892, 22:46–50

Giles-Guzman AD, Alvarez-Borrego S (2000) Vertical attenuation coefficient of photosynthetically active radiation as a function of chlorophyll concentration and depth in case 1 waters. Appl Opt 39:1351–1358

Hardman-Mountford NJ, Richardson AJ, Agenbag JJ, Hagen E, Nykjaer L, Shillington FA, Villacastin C (2003) Ocean climate of the South East Atlantic observed from satellite data and wind models. Prog Oceanogr 59:181–221

Hastie T, Tibshirani R (1990) Generalised additive models. Chapman & Hall, London

Hewitson BC, Crane RG (2002) Self-organizing maps: applications to synoptic climatology. Clim Res 22:13–26

IOC, IHO and BODC (2003) Centenary edition of the GEBCO digital atlas, published on CD-ROM on behalf of the Intergovernmental Oceanographic Commission, and the International Hydrographic Organization as part of the general bathymetric chart of the oceans. British Oceanographic Data Centre, Liverpool

Kohonen T (1997) Self-organizing maps. Springer, Berlin

Kohonen T, Hynninen J, Kangas J, Laaksonen J (1996) SOM_PAK: the self-organizing map program package. Helsinki University of Technology, Laboratory of Computer and Information Science, Technical Report A31, Espoo

Kyewalyanga M, Platt T, Sathyendranath S (1992) Ocean primary production calculated by spectral and broad-band models. Mar Ecol Prog Ser 85:171–185

Legendre L, Michaud J (1999) Chlorophyll *a* to estimate the particulate organic carbon available as food to large zooplankton in the euphotic zone of oceans. J Plankton Res 21:2067–2083

Lett C, Roy C, Levasseur A, Van Der Lingen CD, Mullon C (2006) Simulation and quantification of enrichment and retention processes in the southern Benguela upwelling ecosystem. Fish Oceanogr 15:363–372

Longhurst A (1995) Seasonal cycles of pelagic production and consumption. Prog Oceanogr 36:77–167

Longhurst A, Sathyendranath S, Platt T, Caverhill C (1995) An estimate of global primary production in the ocean from satellite radiometer data. J Plankton Res 17:1245–1271

MathSoft (2001). S-Plus 6 for Windows. Guide to statistics. Insightful Corporation, Seattle, WA

Mitchel-Innes BA (2000) Productivity of dinoflagellate blooms on the west coast of South Africa, as measured by natural fluorescence. S Afr J Mar Sci 22:273–284

Montecino VR, Astoreca R, Alarcón G, Retamal L, Pizarro G (2004) Bio-optical characteristics and primary productivity during upwelling and non-upwelling conditions in a highly productive coastal ecosystem off central Chile (~36° S). Deep-Sea Res II 51:2413–2426

Morel A (1988) Optical modeling of the upper ocean in relation to its biogenous matter content. J Geophys Res 93:10749–10768

Morel A (1991) Light and marine photosynthesis: a spectral model with geochemical and climatological implications. Prog Oceanogr 26:263–306

Morel A, Berthon JF (1989) Surface pigments, algal biomass profiles and potential production of the euphotic layer: relationships reinvestigated in view of remote-sensing applications. Limnol Oceanogr 34:1545–1562

Morel A, Maritorena S (2001) Bio-optical properties of oceanic waters: a reappraisal. J Geophys Res 106: 7163–7180

Morel A, Gentili B, Chami M, Ras J (2006) Bio-optical properties of high chlorophyll Case 1 waters and of yellow-substance-dominated Case 2 waters. Deep-Sea Res I 53: 1439–1459

Nelson DM, Smith WO Jr (1991) Sverdrup revisited: critical depths, maximum chlorophyll levels, and the control of Southern Ocean productivity by the irradiance-mixing regime. Limnol Oceanogr 36:1650–1661

O'Reilly JE, Maritorena S, Mitchell BG, Siegel DA and others (1998) Ocean color chlorophyll algorithms for SeaWiFS. J Geophys Res 103:24937–24953

Parrish RH, Bakun A, Husby DM, Nelson CS (1983) Comparative climatology of selected environmental processes in relation to eastern boundary current pelagic fish reproduction. In: Sharp GD, Csirke J (eds) Proceedings of the Expert Consultation to Examine Changes in Abundance and Species Composition of Neritic Fish Resources, San Jose, Costa Rica, April 1982. FAO Fish Rep 291:731–777

Parsons TR, Maita Y, Lalli CM (1984) A manual of chemical and biological methods for seawater analysis, 14th edn. Pergamon, New York

Patt FS, Barnes RA, Eplee RE, Franz BA and others (2003) Algorithm updates for the fourth SeaWiFS data reprocessing. In: Hooker SB, Firestone ER (eds) SeaWiFS Postlaunch Technical Report Series, Vol 22, NASA Tech Memo 206892. NASA Goddard Space Flight Center, Greenbelt, MD

Platt T, Sathyendranath S (1988) Oceanic primary production: estimation by remote sensing at local and regional scales. Science 241:1613–1620

Platt T, Sathyendranath S (1993) Estimators of primary production for interpretation of remotely sensed data on ocean colour. J Geophys Res 98:14561–14576

Platt T, Sathyendranath S, Caverhill CM, Lewis MR (1988) Ocean primary production and available light: further algorithms for remote sensing. Deep-Sea Res 35:855–879

Probyn TA, Mitchell-Innes BA, Brown PC, Hutchings L, Carter RA (1994) A review of primary production and related processes on the Agulhas Bank. S Afr J Sci 90: 166–173

Richardson AJ, Pfaff MC, Field JG, Silulwane NF, Shillington FA (2002) Identifying characteristic chlorophyll *a* profiles in the coastal domain using an artificial neural network. J Plankton Res 24:1289–1303

Richardson AJ, Silulwane NF, Mitchell-Innes BA, Shillington FA (2003) A dynamic quantitative approach for predicting the shape of phytoplankton profiles in the ocean. Prog Oceanogr 59:301–319

Riley GA (1956) Oceanography of Long Island Sound, 1952–54. 9. Production and utilization of organic matter. Bull Bingham Oceanogr Collect 15:324–343

Sathyendranath S, Platt T (1993) Remote sensing of water-column primary production. ICES Mar Sci Symp 197: 236–243

Sathyendranath S, Longhurst AR, Caverhill CM, Platt T (1995) Regionally and seasonally differentiated primary production in the North Atlantic. Deep-Sea Res 42: 1773–1802

Shannon LJ, Christensen V, Walters CJ (2004a) Modelling stock dynamics in the southern Benguela ecosystem for the period 1978–2002. Afr J Mar Sci 26:179–196

Shannon LJ, Field JG, Moloney CL (2004b) Simulating anchovy–sardine regime shifts in the southern Bengeula ecosystem. Ecol Model 172:269–281

Shannon LV (1985) The Benguela ecosystem. 1. Evolution of the Benguela, physical features and processes. In: Barnes M (ed) Oceanography and marine biology. An annual review, 23. University Press, Aberdeen, p 105–182

Silulwane NF, Richardson AJ, Shillington FA, Mitchell-Innes BA (2001) Identification and classification of vertical chlorophyll patterns in the Benguela upwelling system and Angola–Benguela front using an artificial neural network. In: Pillar SC, Crawford RJM (eds) A decade of Namibian fisheries science. S Afr J Mar Sci 23:37–51

Smith EL (1936) Photosynthesis in relation to light and carbon dioxide. Proc Natl Acad Sci USA 22:504–511

United Nations (2002) Johannesburg Plan of Implementation of the United Nations world summit on sustainable development, Chap 4, para 30. Available at: www.un.org/esa/sustdev/documents/WSSD_POI_PD/English/POIChapter4.htm

Van der Lingen CD, Shannon LJ, Cury P, Kreiner A, Moloney CL, Roux JP, Vaz-Velho F (2006) Resource and ecosystem variability, including regime shifts, in the Benguela Current system. In: Shannon V, Hempel G, Malanotte-Rizzoli P, Moloney C, Woods J (eds) Benguela: predicting a large marine ecosystem. Large marine ecosystems 14. Elsevier, Amsterdam, p 147–185

Editorial responsibility: Alain Vézina, Dartmouth, Nova Scotia, Canada

Submitted: September 5, 2006; Accepted: July 2, 2007
Proofs received from author(s): December 13, 2007